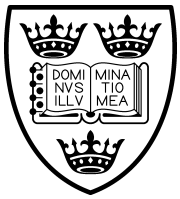
Mechanisms of Carding

Fibres and Hydrodynamics

M. Sc. Mathematical Modelling and Numerical Analysis

Dissertation



Michael Eung-Min Lee

St. John's College

Oxford

September 25, 1997

Abstract

A model for a slender thread or fibre in a slow viscous incompressible fluid is derived. The material of the thread is assumed to have no bending stiffness and to be strictly inextensible. The model is then applied to a simplified industrial situation found in carding, where a thread hangs off a hook. In two limiting cases, perturbation methods give approximate asymptotic solutions, and numerical solutions are found for the general case.

Acknowledgements

I would like to thank Dr. Peter Howell, my university supervisor, for his advice and inspiration throughout the duration of the course, and Dr. Hilary Ockendon for suggesting the topic of the dissertation and for overseeing my progress. The Mathematical Institute, University of Oxford, have kindly provided an industrial bursary, without which I would not have been able to read for this degree. Finally, I am indebted to my parents for their steadfast and continued support.

Contents

1 Introduction **5**

1.1 Industrial Motivation 5

2 The Model **9**

2.1 The Fibre 10

2.2 Fluid Mechanics 10

2.2.1 Inner expansion 10

2.2.2 Outer expansion 12

2.2.3 Matched asymptotics 14

2.2.4 Drag force 17

2.2.5 Effects of inertia 18

2.3 Rotational Forces 18

2.4 The Governing Equations 19

2.4.1 Nondimensional form 21

3 Analysis and Results **22**

3.1 Local Analysis at the Trailing End 22

3.2 Limiting Cases 24

3.2.1 Constant θ 24

3.2.2 Small drag: $0 < \kappa \ll 1$ 25

3.2.3 Small centrifugal force: $\kappa \gg 1$ 26

3.3 General κ 28

3.3.1 Reformulation of problem 28

3.3.2 Comparison of numerical and asymptotic solution 30

3.4 The Hook Problem 31

4 Conclusion **36**

A Computations in Mathematica **39**

A.1 Differential Equations: a shooting method 39

A.2 Differential Equations: the full equations 39

A.3 Differential Equations: the hook 40

List of Figures

1.1 The revolving-flat carding machine 6
1.2 The two mechanisms found in a carding machine 7

2.1 Local cylindrical co-ordinate system 11
2.2 Graphical representation of the variables 14
2.3 The rotating system 19
2.4 A two-dimensional fibre with applied forces 20

3.1 A two-dimesional model of a fibre in a shearing flow. 22
3.2 Two cases for constant θ 25
3.3 A graph plotting the fibre displacement with $\kappa = 0.1$. 26
3.4 A graph of the first-order fibre displacement. 28
3.5 Fibre displacements for varying κ 29
3.6 The height as a function of the nondimensional constant κ 30
3.7 The h against κ, with $\frac{1}{\sqrt{\kappa}}$ the dotted line 31
3.8 Fibres for $\kappa = 10$, $\epsilon = 10^{-5}$, the asymptotic solution is the dotted line. 32
3.9 Fibres for $\kappa = 0.1$, $\epsilon = 10^{-5}$, the asymptotic solution is the dotted line. 33
3.10 A diagram of the hook and fibre 33
3.11 F/N plotted against κ for varying ζ, where ζ is incremented in by $\frac{\pi}{40}$. 34
3.12 F/N plotted against κ for varying ζ, where ζ is incremented in by $\frac{\pi}{40}$. 34
3.13 F/N plotted against κ, for larger angles of attack ζ. 35

Chapter 1

Introduction

The production and processing of textiles involve some of the oldest technologies known to man. Although the processes involved have been refined and made more efficient over the centuries most of the progress has been made empirically. In today's competitive market, such a trial-and-error approach is no longer acceptable. Our ultimate goal is to achieve a real understanding of the underlying physics and thus to pave the way to radical improvements in textile manufacture, using the powerful tools of applied mathematics.

One of the most important and worst understood processes in the production of textiles is the carding process, whereby rough dirty natural fibres are refined to a coherent, smooth web that is suitable for spinning. In this project we give an introduction to some of the elementary mechanisms found in a revolving flat-plate card. We concentrate on the simplest case, namely the motion of a single fibre fixed to a cylinder rotating with a constant angular velocity. From this we find the forces required to hold the fibre onto a hook inclined at a chosen angle.

1.1 Industrial Motivation

Here, we briefly describe the Carding process. It is one of the most important steps in preparing fibres for spinning. When the textile arrives at the spinning mill it is arranged in masses of tufts consisting of entangled fibres. It is necessary to arrange the material in a uniform state in terms of density and thickness, and this is achieved by a "combing" process. Since the original process employed a type of thistle called 'teazle', or in French 'la carde', this stage of textile manufacturing is known as carding.

Industrial advance has lead to the use of continuous carding machines. Revolving-flat plate carding machines, see figure 1.1 have been developed over the past forty five years by Crosrol Ltd, who have also published a concise treatise on the subject [9]. In general the description of this industry is well documented, see e.g. Marsh [19].

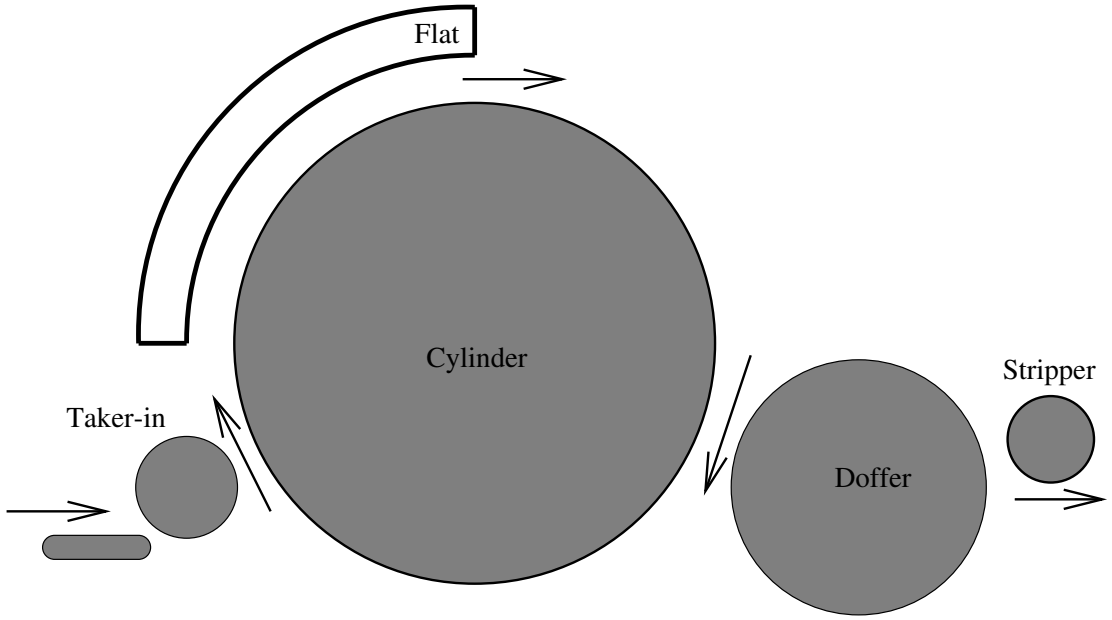


Figure 1.1: The revolving-flat carding machine

There are two mechanisms to consider, carding and stripping, see figure 1.2. In each case the fibres are held to the rotating drum by an attractive force produced by the array of hooks on the cylinder. The more acute the angle made by the hooks with the drum, the stronger this force is. The combined holding forces will also take into consideration the surface speed of the roller.

The entangled fibre masses are fed into the machine by the 'taker-in', during which the tufts are broken down into smaller pieces. The transfer to the 'cylinder' is via the loose trailing back ends. The 'cylinder' has an array of wires that are more dense and travel faster than those on the 'taker-in'. Most of the fibres reside on this drum for several cycles and thus form the 'carding cloth'.

The 'flat' has a surface speed slower than the 'cylinder' and has a combing effect on the fibres on the cylinder. Another purpose of this part of carding is that the flat retains other unwanted objects such as dirt, fluff and short fibres. Next, the fibres move onto the 'doffer', which moves approximately thirty times slower than

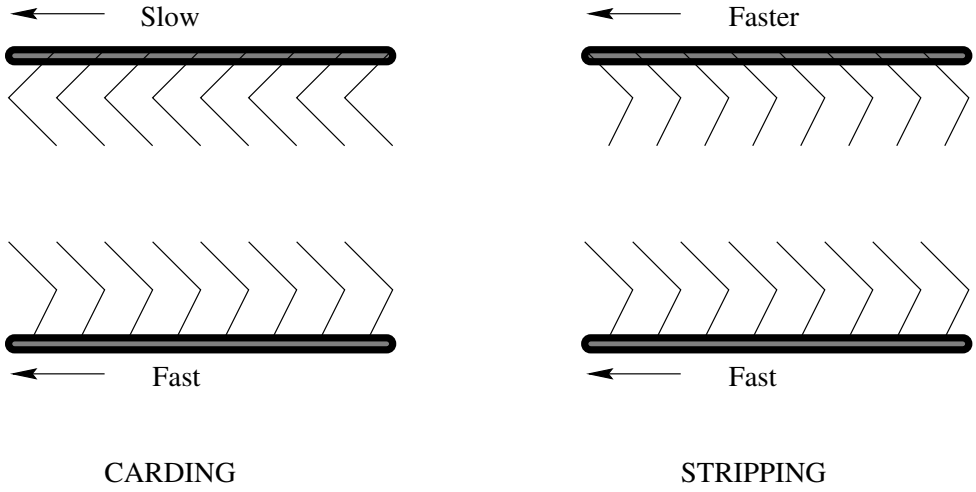


Figure 1.2: The two mechanisms found in a carding machine

the 'cylinder'. In this stage a coherent web is formed from the loose textile, but some fibres are rejected and left on the 'cylinder'. Increasing the 'doffer' speed improves the transfer from the 'cylinder' and leaves a thinner layer of material, but reduces the efficiency of this final stage.

There are a number of principles that are fundamental in understanding the mechanisms involved; the coarseness of the metal wires on the three drums and their surface speed, and the gap between each component. Most of these will depend on the specification of the textile in the machine. The degree of entanglement of the tufts of fibres as the textile enters the machine will be a principle factor. This will depend on length, fineness, bending rigidity, crimping and friction. If the entanglement is too severe fibre breakage will occur during this process. No qualitative work has been done relating saw-tooth wire geometry to fibre properties.

The load on the carding surfaces also has considerable effect. The magnitude of the loading governs the efficiency, cleaning power, mixing and equalising, and hence, the overall productivity. Baturin [3] describes this in detail. The load on the cylinder and the 'doffer' is related by the number of hooks on the respective drums, the centrifugal forces caused by rotation, the entrapment power and fibre capacity of the wires on both surfaces. Baturin also shows that the ratio between load and drum speed govern the transfer between cylinder and doffer.

Aerodynamic forcing plays a major part in the overall process as air is the trans-

port medium between the drums. It is thought that for much of the time the fluid, in the revolving flat plate card, is turbulent. For a single fibre Gradon and Podgorski [13] show how the behaviour of a fibre is affected by the transporting gas, and by its slenderness and initial orientation. The particles quickly accommodate the flow along the fluid streamlines, and with this Gradon and Podgorski model the deposition of fibres on a cylindrical obstacle. There are two other similar papers, but less relevant. One is by Gradon, Podgorski and Gryzbowski [12] where the deposition of stiff and electrically charged particles are estimated. The other by Podgorski and Gradon [20] discusses the motion of a fibre in a laminar gas and its deposition in pipes.

The motion of a mass of fibres is discussed by Shaqfeh and Fredrickson [24], who look at the transport properties of a random array of slender fibres. A two-fluid continuum approach is presented by Sarkar and Lumley [22] and gives numerical results for two-dimensional motion of fibres entering a shear flow. A less relevant paper by Shaqfeh and Koch [23] analyses the motion of particles through a fixed bed of spheres or fibre, and also considers dilute polymer solutions. Terrill [25] looks at a continuum model for a mass of fibres in a fluid for the wet spinning process.

A complicating factor is that irregularities occur in the web produced by the carding machine. Cherkassky [5] examines a simple two-dimensional input-output model of the process, using a random function field to attempt to predict these fluctuations. The model does not use the physics of the smaller scale motions to derive this global process function, but instead uses a heuristic approach.

Chapter 2

The Model

In this chapter we derive the governing equations for a fibre of negligible bending stiffness moving through a viscous fluid under a body force. We make the Stokes flow approximation and use matched asymptotic expansions to derive the drag force exerted by the fluid on the fibre.

The behaviour of solids with small aspect ratios within a fluid field have attracted the attention of a number of previous workers. Batchelor [2] looks at slender particles with arbitrary cross sections, and by neglecting inertia forces, uses a distribution of Stokeslets to represent the body in the 'outer' flow. He finds that a varying cross-section doesn't effect the Stokeslet strength density to leading order. Cox [8] investigates a general theory for the motion of slender bodies in a viscous fluid, and finds the force per unit length on a thread by a logarithmic asymptotic expansion in terms of the aspect ratio of the body. Considering higher order terms terms he also discusses the interaction of two bodies, and that of a body with a wall. Keller and Rubinow [15] briefly review and continue work on slender body theory for slow viscous flow. They employ Stokeslets, just as Batchelor [2] and Lighthill [18] had done in similar situations, which results in an integral equation and ultimately a force density that is in good agreement with Cox's work.

Youngren and Acrivos [26] solve two problems numerically, one of a cylinder translating parallel to its axis, and second for a freely suspended cylinder. Their results showed good agreement with Cox [8]. Dabros [10] also considers numerical solutions for a fibre near a solid wall. Other related works include the analytical findings of Chwang and Wu [6] who look at more general bodies in a slow flow, and Lighthill [18] who models the motion of micro-organisms. Hinch [14], Barshinger [4] and Terrill [25]

both use these calculations to model different, and more specific physical situations, including those found in physiology and the textiles industry.

2.1 The Fibre

The fibre has length l and cross-sectional radius a. The position of the centre line of the fibre is denoted by a dimensional vector $\mathbf{x} = \mathbf{X}(s)$ where s is arc length. Dashes and dots will be used to represent derivatives with respect to arc length and time respectively. Since s denotes arc length and the fibre is assumed to be strictly inextensible,

$$\mathbf{X}' \cdot \mathbf{X}' = 1, \tag{2.1}$$

$$\text{and hence} \quad \dot{\mathbf{X}}' \cdot \mathbf{X}' = 0. \tag{2.2}$$

An external force per unit length $\mathbf{f}$ acting on the fibre induces a tension $T(s,t)$, to preserve arc length, i.e. an internal resistive force. The balance between these reads

$$(T\mathbf{X}')' + \mathbf{f} = \mathbf{0}. \tag{2.3}$$

2.2 Fluid Mechanics

The air interacting with the fibres will be modelled as a homogeneous incompressible fluid, and this is accurate if the flow is sufficiently sub-sonic, for example the Mach number is less than 0.7, see Liepmann and Roshko [17]. As in Batchelor [2], Cox [8], and Keller and Rubinow [15], we consider a slender cylinder, such that $\varepsilon = \frac{a}{l} \ll 1$. The fluid mechanics near the body behaves essentially as a slow viscous flow around an infinite cylinder. In the outer solution the fibre is treated as an infinitesimally thin body: a line singularity. A restriction we need is that curvature doesn't exceed $O(l^{-1})$. For additional simplicity, we assume the fibre is stationary in a frame rotating with the cylinder.

2.2.1 Inner expansion

In the inner region, considering length scales of either l or a, inertia is neglected so the motion of the fluid is governed by the stokes equations:

$$\nabla^2 \mathbf{u} = \mu \nabla p \quad \text{and} \quad \nabla \cdot \mathbf{u} = 0, \tag{2.4}$$

where μ is the viscosity, $\mathbf{u}$ is the fluid velocity and p is the pressure field. Consider the neighbourhood of a point P on the fibre, corresponding to $s = s_p$. Rescaling locally,

$$\mathbf{x} = \mathbf{X}(s_P) + a\bar{\mathbf{x}}, \tag{2.5}$$

where as before a is the fibre radius. We nondimensionalise the fluid velocity $\mathbf{u}$ and pressure p with

$$\mathbf{u} = U\bar{\mathbf{u}}, \quad p = \frac{\mu U}{a}\bar{p} \tag{2.6}$$

to get

$$\nabla^2\bar{\mathbf{u}} = \nabla\bar{p} \quad \text{and} \quad \nabla\cdot\bar{\mathbf{u}} = 0, \tag{2.7}$$

using a set of Cartesian axes, $(\mathbf{i}_1, \mathbf{i}_2, \mathbf{i}_3)$ where $\mathbf{i}_1$ lies tangential to C as in figure (2.1). The inner variable, denoted with bars, are of order unity. Relative to these axes, due

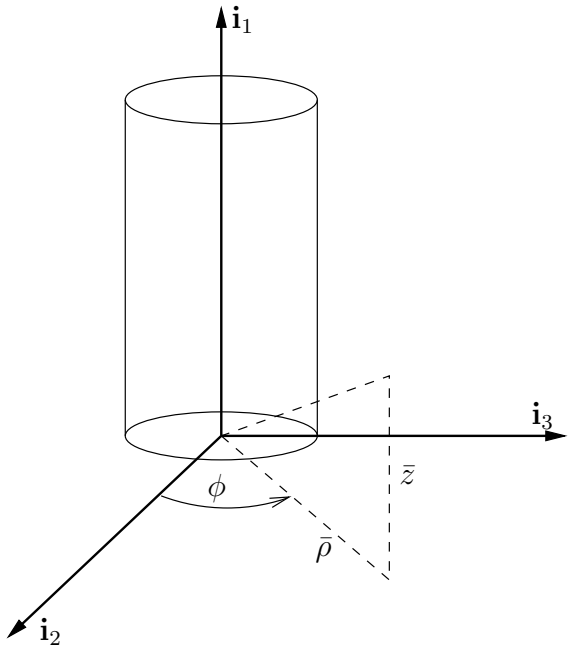


Figure 2.1: Local cylindrical co-ordinate system

to the geometry of the body, a cylindrical polar system, $(\bar{r}, \bar{\phi}, \bar{z})$, is employed with $\bar{x}_1 = z$, $\bar{x}_2 = \bar{r}\cos\phi$, $\bar{x}_3 = \bar{r}\sin\phi$, and $\bar{r} = \sqrt{x_2^2 + x_3^2}$. A no-slip condition $\bar{\mathbf{u}} = 0$, is applied on the surface of the cylinder, which in the neighbourhood of P, may be expressed in the form

$$\bar{r} = 1 + O(s - s_P) = 1 + O(\varepsilon). \tag{2.8}$$

For a varying cross section, this formulation can be easily modified using a radius function that varies with arc length. This is computed explicitly by Cox [8] and Batchelor [2], and the latter found that general slender body shapes do not effect the leading order terms of the asymptotic approximation.

We pose the following regular perturbation expansions:

$$\begin{aligned} \bar{\mathbf{u}} &= \bar{\mathbf{u}}_{\mathbf{0}} + \varepsilon \bar{\mathbf{u}}_{\mathbf{1}} + O(\varepsilon^2), \\ \bar{p} &= \bar{p}_0 + \varepsilon \bar{p}_1 + O(\varepsilon^2). \end{aligned} \tag{2.9}$$

Thus, $(\bar{\mathbf{u}}_{\mathbf{0}}, \bar{p}_0)$ satisfies the governing equations for $(\bar{\mathbf{u}}, \bar{p})$ and the no-slip condition on $\bar{r} = 1$. Now, from the well-documented solutions for the stream function ψ, which is governed by the homogeneous biharmonic operator, a general solution that tends to infinity most slowly as $\mathbf{x} \to \infty$ with no-slip boundary conditions is found to be,

$$\psi = \frac{A}{2}\left[2r \ln r - r + \frac{1}{r}\right] \sin\phi, \tag{2.10}$$

see Rosenhead [21] or Batchelor [1]. Therefore, the velocity is as follows,

$$(\bar{u}_0)_r = \frac{A}{2}\left[1 - \frac{1}{\bar{r}^2} - 2\ln\bar{r}\right]\cos\phi, \tag{2.11}$$

$$(\bar{u}_0)_\phi = \frac{A}{2}\left[1 - \frac{1}{\bar{r}^2} + 2\ln\bar{r}\right]\sin\phi, \tag{2.12}$$

$$(\bar{u}_0)_z = B\ln\bar{r}, \tag{2.13}$$

$$\bar{p}_0 = \frac{2A}{r}\cos\phi. \tag{2.14}$$

Here, A and C are arbitrary constants which will be found by matching with the outer solution. Choosing to work in a Cartesian frame, the leading order velocity is transformed into,

$$\begin{aligned} \bar{\mathbf{u}}_{\mathbf{0}} = {} & \mathbf{i_1} B \ln\bar{r} + \mathbf{i_2}\frac{A}{2}\left[2\ln\bar{r} - \left(1 - \frac{1}{\bar{r}^2}\right)(\cos^2\phi - \sin^2\phi)\right] \\ & - \mathbf{i_3} A\left(1 - \frac{1}{\bar{r}^2}\right)\sin\phi\cos\phi. \end{aligned} \tag{2.15}$$

2.2.2 Outer expansion

The outer expansion variables take the form:

$$\begin{aligned} \mathbf{x} &= \frac{1}{\varepsilon}\bar{\mathbf{x}}, \\ \mathbf{u}(\mathbf{x}) &= \bar{\mathbf{u}}(\bar{\mathbf{x}}) = \mathbf{u_0} + \varepsilon \mathbf{u_1} + O(\varepsilon^2), \\ p(\mathbf{x}) &= \frac{1}{\varepsilon}\bar{p}(\bar{\mathbf{x}}) = p_0 + \varepsilon p_1 + O(\varepsilon^2). \end{aligned} \tag{2.16}$$

The leading-order flow field, $(\mathbf{u_0}, p_0)$, approximates the cylinder by a line force and uses the undisturbed flow as the far field. The line force is a distribution of Stokeslets, which are singularities in Stokes flow representing the effect of a force applied to the fluid at a point, see Lighthill [18], and Chwang and Wu [6]. Incorporating a point force $\mathbf{F}$ into the Stokes equations, using a Dirac delta-function, we obtain

$$-\nabla p + \nabla^2 \mathbf{u} + \mathbf{F}\delta(\mathbf{x}) = \mathbf{0}, \tag{2.17}$$

$$\nabla \cdot \mathbf{u} = \mathbf{0}. \tag{2.18}$$

Eliminating $\mathbf{u}$,

$$\nabla^2 p = \nabla \cdot [\mathbf{F}\delta(\mathbf{x})], \tag{2.19}$$

$$\text{and hence} \quad p = -\nabla \cdot \left[\frac{\mathbf{F}}{4\pi\hat{r}}\right]. \tag{2.20}$$

Here, $\hat{r}$ is the modulus of the displacement vector, $\hat{r} = \sqrt{x_1^2 + x_2^2 + x_3^2}$. This is the classical dipole field for an external force $\mathbf{F}$ applied to the fluid at $\hat{r} = 0$.

As an example, suppose $\mathbf{F} = F\mathbf{i_1}$, so that the pressure field is $\frac{Fx_1}{4\pi r^3}$. Then (2.17) gives,

$$\nabla^2 \mathbf{u} = \frac{F}{4\pi}\left(\frac{1}{\hat{r}^3} - \frac{3x_1^2}{\hat{r}^3}, -\frac{3x_1x_2}{\hat{r}^5}, -\frac{3x_1x_3}{\hat{r}^5}\right). \tag{2.21}$$

This can be solved using Lighthill's [18] technique for determining functions whose Laplacian is a given homogeneous harmonic function. Hence a solution corresponding to the force in the $\mathbf{i_1}$ direction is:

$$\mathbf{u} = \frac{F}{8\pi}\left(\frac{x_1^2 + \hat{r}^2}{\hat{r}^3}, \frac{x_1x_2}{\hat{r}^3}, \frac{x_1x_3}{\hat{r}^3}\right). \tag{2.22}$$

Now for arbitrary $\mathbf{F}$, we generalise this solution to,

$$\mathbf{u} = \frac{1}{8\pi}\left[\frac{\mathbf{F}}{\hat{r}} + \frac{(\mathbf{F}\cdot\mathbf{x})\mathbf{x}}{\hat{r}^3}\right] = \frac{F_j}{8\pi}\left[\frac{\delta_{ij}}{\hat{r}} + \frac{x_i x_j}{\hat{r}^3}\right]. \tag{2.23}$$

This is the general velocity field for a Stokeslet. For the purposes of modelling a line force, we use an array of Stokeslets with density $\boldsymbol{\alpha}(s)$. The leading-order terms of the outer solution are thus,

$$\mathbf{u_0} = \mathbf{U} + \int_0^1 \left[\frac{\boldsymbol{\alpha}}{R} + \frac{(\boldsymbol{\alpha}\cdot\mathbf{R})\mathbf{R}}{R^3}\right] d\hat{s}, \tag{2.24}$$

$$p_0 = P + 2\int_0^1 \left[\frac{\boldsymbol{\alpha}\cdot\mathbf{R}}{R^3}\right] d\hat{s}, \tag{2.25}$$

defining the solution field at infinity to be $(\mathbf{U}, P)$, $\mathbf{R}(\hat{s}) = \mathbf{x} - \mathbf{X}(\hat{s})$, and $R = |\mathbf{R}|$.

2.2.3 Matched asymptotics

A combination of 'outer' and 'inner' solutions is required to find a composite solution. In this case our leading-order terms are considered, and thus, we simply require that the behaviour of the 'inner' solution as $\bar{r} \to \infty$ agrees with that of the 'outer' solution as $r \to 0$. This form of matching is specific to leading order approximations.

Inner Expansion of Outer Expansion

To determine the integration constants and the Stokeslets density, we evaluate (2.24) in the limit $\mathbf{x} \to \mathbf{X}$. From Keller and Rubinow [15], the following procedure is adopted,

$$\begin{aligned} \mathbf{I}(\mathbf{x}) &= \int_0^1 \left[\frac{\boldsymbol{\alpha}(\hat{s})}{R} + \frac{(\boldsymbol{\alpha}(\hat{s}) \cdot \mathbf{R})\mathbf{R}}{R^3} \right] d\hat{s} \\ &= \int_{-s}^{1-s} \left[\frac{\boldsymbol{\alpha}(s+t)}{R} + \frac{(\boldsymbol{\alpha}(s+t) \cdot \mathbf{R})\mathbf{R}}{R^3} \right] dt \quad \text{with} \quad \hat{s} = s + t. \end{aligned} \tag{2.26}$$

Now set $\mathbf{x} = \mathbf{X} + \mathbf{r}$, where $\mathbf{r} \cdot \mathbf{X_s} = 0$ because $\mathbf{X}$ is the point on C nearest to $\mathbf{x}$, and $\mathbf{X_s}$ is the unit vector tangent to C. Then

$$\mathbf{R}(t, \mathbf{r}) = \mathbf{x}(s) - \mathbf{X}(x + t) = \mathbf{r} + \mathbf{X}(s) - \mathbf{X}(s + t). \tag{2.27}$$

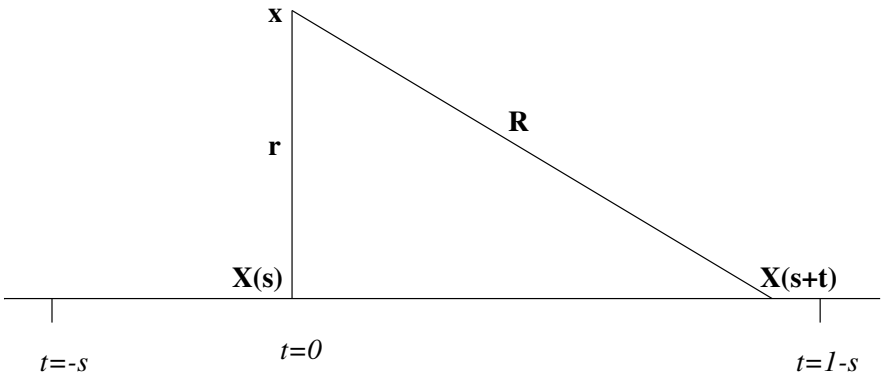


Figure 2.2: Graphical representation of the variables

Letting $\mathbf{R_0} = \mathbf{X}(s) - \mathbf{X}(s + r)$, we find $R^2 = r^2 + 2\mathbf{R_0} \cdot \mathbf{r} + R_0^2 = r^2 + t^2c^2$, where $c^2(t, \mathbf{r}) = t^{-2}(2\mathbf{R_0} \cdot \mathbf{r} + \mathbf{R_0}^2)$. Upon examination of the integrand in (2.26), singular behaviour occurs when $t = 0$ and $\mathbf{r} \to 0$. Therefore, it is important to analyse c^2 when

$0 < t \ll 1$. Expanding $\mathbf{x_0}(s+t)$ in a Taylor series in t, and using this to expand $\mathbf{R_0}$ with $\mathbf{X_s}(s) = \mathbf{i_1}(s)$, $c^2(t, \mathbf{r})$ becomes $1 - \mathbf{r} \cdot \mathbf{i_1} + O(t)$.

The $\frac{\boldsymbol{\alpha}(s+t)}{R}$ component of the integrand in (2.26) has convergence problems, so we isolate the divergent part by writing

$$\begin{aligned} \int_{-s}^{1-s} \left[\frac{\boldsymbol{\alpha}(s+t)}{R}\right] dt &= \int_{-s}^{1-s} \left[\frac{\boldsymbol{\alpha}(s+t)}{\sqrt{r^2+t^2c^2}} - \left(\frac{\boldsymbol{\alpha}}{c}\right)_{t=0} \frac{1}{\sqrt{r^2+t^2}}\right] dt \\ &\quad + \left(\frac{\boldsymbol{\alpha}}{c}\right)_{t=0} \int_{-s}^{1-s} \frac{dt}{\sqrt{r^2+t^2}}. \end{aligned} \tag{2.28}$$

The second integral on the right side of (2.28), as $r \to 0$, behaves like $-2\ln r$. Using $c(0,0) = 1$, $(\boldsymbol{\alpha})_{t=0} = \boldsymbol{\alpha}(s)$, the exact term is $-2\boldsymbol{\alpha}(s)\ln r$. Subtracting this from the left integral in (2.28) we find that the resulting difference has a finite limit as $r \to 0$. Alternatively, by setting $r = 0$ in the first of the left hand integrals and evaluating the second, the finite part can be expressed as

$$\int_{-s}^{1-s} \left[\frac{\boldsymbol{\alpha}(s+t)}{R_0} - \frac{\boldsymbol{\alpha}}{|\ t\ |}\right] dt + \boldsymbol{\alpha}(s)\ln[4s(1-2)]. \tag{2.29}$$

Similarly,

$$\begin{aligned} \int_{-s}^{1-s} \left[\frac{(\boldsymbol{\alpha}\cdot\mathbf{R})\mathbf{R}}{\mathbf{R}^3}\right] dt &= \int_{-s}^{1-s} \left[\frac{1}{(r^2+t^2c^2)^{3/2}} \sum_{j=0}^{2} \frac{t^j}{j!}\frac{d^j}{dt^j}\left(\frac{(\boldsymbol{\alpha}\cdot\mathbf{R})\mathbf{R}}{c^3}\right)_{t=0}\right] dt \\ + \int_{-s}^{1-s} \left[\frac{(\boldsymbol{\alpha}\cdot\mathbf{R})\mathbf{R}}{(r^2+t^2c^2)^{3/2}} - \frac{1}{(r^2+t^2c^2)(3/2)} \sum_{j=0}^{2} \frac{t^j}{j!}\frac{d^j}{dt^j}\left(\frac{(\boldsymbol{\alpha}\cdot\mathbf{R})\mathbf{R}}{c^3}\right)_{t=0}\right] dt. \end{aligned} \tag{2.30}$$

The second integral is finite and the first is evaluated exactly using the following,

$$\frac{d}{dt}\left[\frac{(\alpha\cdot\mathbf{R})\mathbf{R}}{c^3}\right]_{t=0} = O(r) \tag{2.31}$$

$$\int_{-s}^{1-s} \frac{t}{(r^2+t^2)^{3/2}} dt = \frac{1}{r} + \frac{1}{s(s-1)} \tag{2.32}$$

$$\frac{1}{2}\frac{d^2}{dt^2}\left[\frac{(\alpha\cdot\mathbf{R})\mathbf{R}}{c^3}\right]_{t=0} = (\alpha\cdot\mathbf{i_1})\mathbf{i_1} + O(r) \tag{2.33}$$

$$\int_{-s}^{1-s} \frac{t^2}{(r^2+t^2)^{3/2}} dt = -2\ln r + \ln 4s(1-s) - 2 + O(r^2). \tag{2.34}$$

Hence the divergent part for this particular integral in (2.30), is $-2\mathbf{i_1}(\alpha\cdot\mathbf{i_1})\ln r$. The finite part is defined as,

$$\lim_{r\to 0}\int_{-s}^{1-s}\frac{(\boldsymbol{\alpha}\cdot\mathbf{R})\mathbf{R}}{R^3}dt+2\alpha_1\mathbf{i_1}\ln r=\int_{-s}^{1-s}\left[\frac{(\boldsymbol{\alpha}(s+t)\cdot\mathbf{R_0})\mathbf{R_0}}{R_0^3}-\frac{t^2\alpha_1\mathbf{i_1}}{|t|^3}\right]dt$$
$$+2(\hat{\mathbf{r}}\cdot\boldsymbol{\alpha})\hat{\mathbf{r}}+\alpha_1\mathbf{i_1}(\ln[4s(1-s)]-2), \quad (2.35)$$

where $\hat{\mathbf{r}}$ is the unit vector $\frac{\mathbf{r}}{|\mathbf{r}|}$.

Now we have enough information to expand the outer solution (2.24) as $r\to 0$:

$$\mathbf{u}(\mathbf{x})\sim\mathbf{U}(s)-[4\alpha_1(s)\mathbf{i_1}+2\alpha_2(s)\mathbf{i_2}+2\alpha_3(s)\mathbf{i_3}]\ln r+\mathbf{u_f}(s), \quad (2.36)$$

where $\mathbf{u_f}(s)$ is the finite component of the integral in (2.24), $\mathbf{U}(s)=\mathbf{U}[\mathbf{X}(s)]$ and $\boldsymbol{\alpha}=(\alpha_1,\alpha_2,\alpha_3)^T$. Here, $\mathbf{u_f}(s)$ is the velocity disturbance at $\mathbf{X}$ due to the thread outside a neighbourhood of $\mathbf{X}$. It is defined as,

$$\mathbf{u_f}=\lim_{r\to 0}\left[\int_0^1\left(\frac{\boldsymbol{\alpha}}{R}+\frac{(\boldsymbol{\alpha}\cdot\mathbf{R})\mathbf{R}}{R^3}\right)d\hat{s}+[4\alpha_1(s)\mathbf{i_1}+2\alpha_2(s)\mathbf{i_2}+2\alpha_3(s)\mathbf{i_3}]\ln r\right], \quad (2.37)$$

which we know from our previous calculations to be finite.

Outer expansion of inner expansion

Expanding the 'inner' solution as (2.15) $\bar{\mathbf{r}}\to\infty$ we find

$$\bar{\mathbf{u}}\sim\mathbf{i_1}B\ln\bar{r}+\mathbf{i_2}\frac{A}{2}\left[2\ln\bar{r}-(\cos^2\phi-\sin^2\phi)\right]-\mathbf{i_3}A\sin\phi\cos\phi. \quad (2.38)$$

Matching

Matching between the 'inner' and 'outer' solutions is achieved by equating (2.38) with (2.36). The coefficients of $\ln r$ are

$$B\mathbf{i_1}+A\mathbf{i_2}=[4\alpha_1\mathbf{i_1}+2\alpha_2\mathbf{i_2}+2\alpha_3\mathbf{i_3}], \quad (2.39)$$

which gives $B=-4\alpha_1$, $A=-2\alpha_2$ and $\alpha_3=0$. The order unity terms give the following equation,

$$\mathbf{U}+\mathbf{u_f} \;=\; -\mathbf{i_2}\frac{A}{2}(\cos^2\phi-\sin^2\phi)-\mathbf{i_3}A\sin\phi\cos\phi. \quad (2.40)$$

Thus,

$$2\ln\bar{r}\mathbf{U}+\mathbf{u_f}-\alpha_2\mathbf{i_2}(\cos^2\phi-\sin^2\phi)-2\alpha_3\mathbf{i_3}\sin\phi\cos\phi=\mathbf{0}. \quad (2.41)$$

Considering the expression for $\mathbf{u_f}$ from (2.37) this is an integral equation for $\boldsymbol{\alpha}$, and can be rearranged by evaluating the different Cartesian components separately, recombining them to give,

$$[2\mathbf{I} - \mathbf{i_1}(\mathbf{i_1})^T]\{\mathbf{U} + \alpha_2\mathbf{i_2}(\cos^2\phi - \sin^2\phi) - 2\alpha_2\mathbf{i_3}\sin\phi\cos\phi + \mathbf{u_f}\} = \mathbf{0}. \tag{2.42}$$

Finding the sum of (2.31) and (2.35) allows us to express $\mathbf{u_f}$ as an integral:

$$[2\mathbf{I} - \mathbf{i_1}(\mathbf{i_1})^T]\left(\mathbf{U} + \alpha_2\mathbf{i_2} + \boldsymbol{\alpha}\ln[4s(1-s)] + \int_{-s}^{1-s}\left[\frac{\alpha(s+t)}{R_0} - \frac{\boldsymbol{\alpha}(s)}{|\,t\,|} + \frac{[\mathbf{R_0}\cdot\boldsymbol{\alpha}(s+t)]\mathbf{R_0}}{R_0^3} - \frac{\alpha_1(s)\mathbf{i_1}t^2}{|\,t\,|^3}\right]dt + \alpha_1(s)\mathbf{i_1}[\ln(4s(1-s)) - 2]\right) = \mathbf{0}, \tag{2.43}$$

$\mathbf{I}$ being the identity matrix and $\mathbf{i_1}(\mathbf{i_1})^T$ a square matrix, or tensor, of the same order as $\mathbf{I}$. Keller and Rubinow [15], use an iterative method to find $\boldsymbol{\alpha}$, and Cox [8] finds the same leading-order term $\boldsymbol{\alpha_0}$, but uses an asymptotic expansion for $\boldsymbol{\alpha}$ in $\ln\varepsilon$:

$$\boldsymbol{\alpha} \sim \frac{1}{\ln\frac{1}{\varepsilon}}\boldsymbol{\alpha_0} + \frac{1}{(\ln\frac{1}{\varepsilon})^2}\boldsymbol{\alpha_1} + O\left(\left[\frac{1}{\ln\frac{1}{\varepsilon}}\right]^3\right) \tag{2.44}$$

where,

$$\boldsymbol{\alpha_0} = [2\mathbf{I} - \mathbf{i_1}(\mathbf{i_1})^T]\mathbf{U}. \tag{2.45}$$

2.2.4 Drag force

The Stokeslet, a singular point force, which without loss of generality we locate at the origin, is defined for our nondimensional case as

$$\mathbf{f_s} = 8\pi\boldsymbol{\alpha}\delta(\mathbf{x}), \tag{2.46}$$

where $\boldsymbol{\alpha}$ is a constant vector characterises the strength in magnitude and direction, see Chwang [6].

So the drag force per unit length of the cylinder $\mathbf{D}$ is,

$$\mathbf{D} \sim -\frac{8\pi\boldsymbol{\alpha_0}}{\ln\varepsilon} + O\left(\left[\frac{1}{\ln\frac{1}{\varepsilon}}\right]^2\right) \tag{2.47}$$

as $\boldsymbol{\alpha}$ is the Stokeslet force density.

2.2.5 Effects of inertia

So far we have considered a slow viscous fluid governed by the Stokes equations, which neglects the inertia terms in the Navier-Stokes equations. Khayat and Cox [16] studied these effects on the motion of long slender bodies, continuing in the spirit of the work of Cox [8]. Using matched asymptotics, with a logarithmic expansion in terms of the aspect ratio, the drag force per unit length is found, which to leading order is the same as our slow flow approximation. We have assumed the Reynolds number Re, based on the cross-sectional radius is small. However, this result is only valid when the second term in the asymptotic expansion of the drag force is smaller than the first as $\varepsilon \to 0$ which means that,

$$\left|\frac{\ln Re - \ln \varepsilon}{(\ln \varepsilon)^2}\right| \ll \left|\frac{1}{\ln \varepsilon}\right|, \tag{2.48}$$

$$\tag{2.49}$$

and therefore our results are valid when

$$Re < \varepsilon^{1-\delta}, \tag{2.50}$$

where δ is a fixed positive constant much smaller than unity. An expression which is valid for all ε and Re as ε, $Re \to 0$ is found by Khayat and Cox [16] where the leading-order term is considerably different from (2.45). Such effects would have to be included if we wished to consider stability of our steady solution.

2.3 Rotational Forces

We suppose the fibre is fixed in a frame rotating with the drum. In general, the force on a mass m at position $\mathbf{x}$ in a frame rotating with angular velocity $\boldsymbol{\omega}$ is

$$\mathbf{R} = m(\ddot{\mathbf{x}} + \dot{\boldsymbol{\omega}} \wedge \mathbf{x} + 2\boldsymbol{\omega} \wedge \dot{\mathbf{x}} + \boldsymbol{\omega} \wedge (\boldsymbol{\omega} \wedge \mathbf{x})). \tag{2.51}$$

Since the fibre is fixed, the only body force it feels is the centrifugal force per unit length $\mathbf{R} = \rho a^2 \boldsymbol{\omega} \wedge (\boldsymbol{\omega} \wedge \mathbf{x})$, where ρ is the fibre density. More precisely, ρ is the difference between the fibre density and the density of air, but we expect the latter to be negligible.

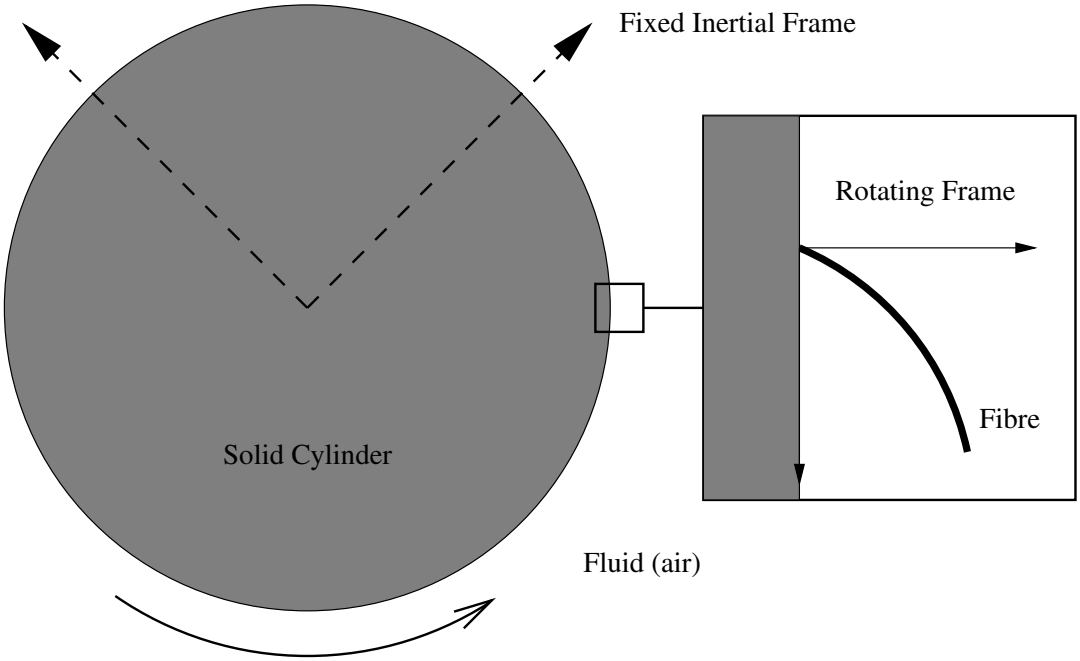


Figure 2.3: The rotating system

2.4 The Governing Equations

The governing equations for a steady situation are derived from a balance between tension, centrifugal force and viscous drag, which reads

$$(T\mathbf{X}')' + \frac{8\pi\mu}{\ln\frac{1}{\varepsilon}}[2\mathbf{I} - \mathbf{X}'(\mathbf{X}')^T]\mathbf{U} + \mathbf{R} = 0, \tag{2.52}$$

along with the inextensibility constraint that the modulus of $\mathbf{X}'$ is 1. We simplify the problem by supposing that the fibre moves in just two dimensions, that $\mathbf{U}$ is the simple shear flow $\mathbf{U} = (yU_d, 0, 0)^T$, and that the radius of the drum is much bigger than l. This last assumption means that the Centrifugal force can be approximated by $\mathbf{R} = \rho a^2\Omega^2 r(0, 0, 1)^T$. Here r is the drum radius, Ω is the angular velocity of the drum, and U_d the gradient of the fluid's velocity profile. The unidirectional 'Couette' flow, which is a solution to the full Navier-Stokes equations, is found to be stable up to a Reynolds number of about 80, see Drazin [11]. An angle-arc-length formulation, with

$$\frac{dX}{ds} = \cos\Theta, \quad \frac{dY}{ds} = \sin\Theta, \tag{2.53}$$

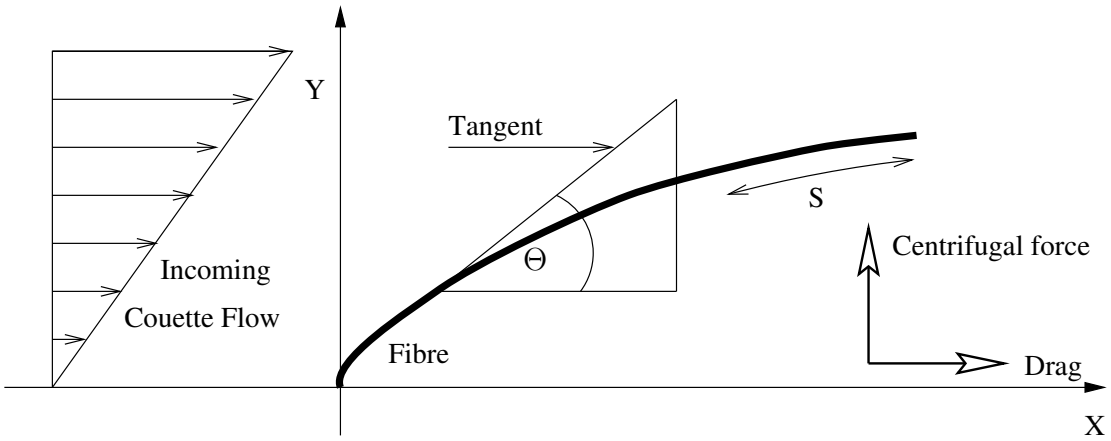


Figure 2.4: A two-dimensional fibre with applied forces

and

$$(T\mathbf{X}')' = \left[T\begin{pmatrix}\cos\Theta\\ \sin\Theta\end{pmatrix}\right]' = T'\begin{pmatrix}\cos\Theta\\ \sin\Theta\end{pmatrix} + T\Theta'\begin{pmatrix}-\sin\Theta\\ \cos\Theta\end{pmatrix} = T'\mathbf{X}' + \Theta' T\mathbf{X}'' \quad (2.54)$$

gives the governing equations,

$$\frac{dT}{dS} + DY\cos\Theta + R\sin\Theta = 0 \quad (2.55)$$

in the $\mathbf{X}'$ direction,

$$T\frac{d\Theta}{dS} - 2DY\sin\Theta + R\cos\Theta = 0 \quad (2.56)$$

in the $\mathbf{X}''$ direction, and one of (2.53),

$$\frac{dY}{dS} - \sin\Theta = 0, \quad (2.57)$$

to close the system. Here D is the drag term $D = 8\pi\mu U_d/\ln\frac{1}{\varepsilon}$ and $R = \rho a^2\Omega^2 r$. There are two boundary conditions. One fixes one end of the fibre, and the other is a force balance at the free end:

$$Y(0) = 0 \quad \text{and} \quad T(l) = 0. \quad (2.58)$$

2.4.1 Nondimensional form

We nondimensionalise (2.55) - (2.57), using $T = lRt$, $Y = ly$, $S = ls$, and $\Theta = \theta$. Our dimensionless parameter is

$$\kappa = \frac{Dl}{R} = \frac{8\pi\mu U_d l}{\rho\Omega^2 a^2 r \ln\frac{1}{\varepsilon}}, \tag{2.59}$$

a ratio between viscous drag and Centrifugal force, and the dimensionless equations are:

$$\frac{dt}{ds} + \kappa y\cos\theta + \sin\theta = 0, \tag{2.60}$$

$$t\frac{d\theta}{ds} - 2\kappa y\sin\theta + \cos\theta = 0, \tag{2.61}$$

$$\frac{dy}{ds} - \sin\theta = 0, \tag{2.62}$$

with

$$t(1) = 0 \quad \text{and} \quad y(0) = 0. \tag{2.63}$$

The system seems to be ill-posed as we have two boundary conditions for three coupled differential equations. In the next chapter we shall see, by using local analysis, that the singularity in (2.61) at $s = 1$ gives the third condition for θ, making this a well-posed problem, although a full analysis of the governing equations has not been done to show this. If $y(1) = h$, where h is height of the fibre from the solid boundary at the trailing end, then

$$\theta(1) = \operatorname{arccot}(2h\kappa) \tag{2.64}$$

is sufficient to eliminate the end point singularity.

Chapter 3

Analysis and Results

From the nondimensional governing equations (2.60) - (2.62), we find the fibre's displacement for varying κ. There are two limiting cases where we apply perturbation analysis, i.e. where either viscous drag, or Centrifugal forces dominate, which correspond to $\kappa \gg 1$ and $\kappa \ll 1$ respectively. In the general case numerical results are found and are in good agreement with the asymptotic results. After considering a fibre on a rotating cylinder, we then find the forces that hold a fibre to a hook with varying angle of attack.

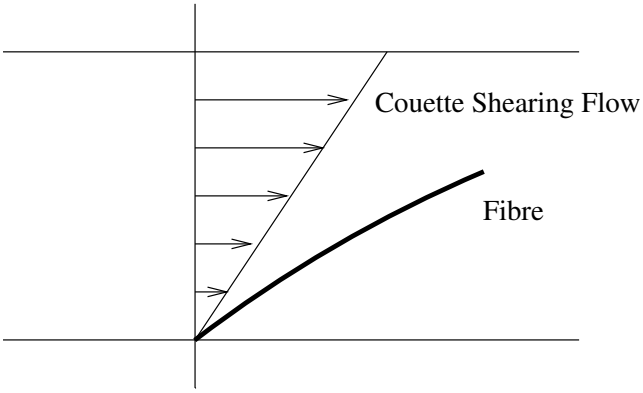


Figure 3.1: A two-dimesional model of a fibre in a shearing flow.

3.1 Local Analysis at the Trailing End

It is necessary to examine the region near $s = 1$ since the system (2.60) - (2.62) is singular there, due to the tension being zero. From this local analysis we find

the boundary conditions needed to solve the full equations computationally. Taking Taylor expansions about $s = 1$ for t, θ, and y, we have

$$\begin{aligned} t(s) &= \sum_{n=0}^{\infty} \frac{t^{(n)}(1)(-\epsilon)^n}{n!}, \quad \theta(s) = \sum_{n=0}^{\infty} \frac{\theta^{(n)}(1)(-\epsilon)^n}{n!}, \\ y(s) &= \sum_{n=0}^{\infty} \frac{y^{(n)}(1)(-\epsilon)^n}{n!}, \end{aligned} \tag{3.1}$$

setting $s = 1 - \epsilon$ with $0 < \epsilon \ll 1$. Now, substituting into (2.60) - (2.62) with the boundary conditions $t(1) = 0$, $\theta(1) = \operatorname{arccot}(2h\kappa)$, and $y(1) = h$ say, we find the following, for order unity:

$$t' + \kappa y \cos\theta + \sin\theta = 0, \tag{3.2}$$

$$t\theta' - 2y\kappa \sin\theta + \cos\theta = 0,$$

$$y' - \sin\theta = 0, \tag{3.3}$$

and order ϵ:

$$t'' + \kappa[y' \cos\theta - y\theta' \sin\theta] + \theta' \cos\theta = 0, \tag{3.4}$$

$$t\theta'' - 2\kappa[y' \sin\theta + y\theta' \cos\theta] + t'\theta' - \theta' \sin\theta = 0, \tag{3.5}$$

$$y'' - \theta' \cos\theta = 0, \tag{3.6}$$

thus giving the asymptotic expansions:

$$t \sim \epsilon \frac{1 + 2(h\kappa)^2}{\sqrt{1 + 4(h\kappa)^2}} + \epsilon^2 \left(2h\kappa(4\kappa - 3) - \frac{3h\kappa^2}{1 + 3h^2\kappa^2} - \frac{8h^3\kappa^4}{1 + 4h^2\kappa^2} \right) \tag{3.7}$$

$$\theta \sim \operatorname{arccot}(2\kappa h) + \epsilon \frac{\kappa}{(1 + 3h^2\kappa^2)(\sqrt{1 + 4h^2\kappa^2})} \tag{3.8}$$

$$y \sim h - \epsilon \frac{1}{\sqrt{1 + 4(h\kappa)^2}} - \epsilon^2 \frac{2h\kappa^2}{(1 + 3h^2\kappa^2)(1 + 4h^2\kappa^2)}. \tag{3.9}$$

This demonstrates that there is a one-parameter family of solutions (parametrised by h) satisfying $t = 0$ at $s = 1$. The remaining parameter h is fixed by imposing $y(0) = 0$. In practice when solving (2.60) - (2.62) numerically we use (3.7) - (3.9) up to $O(\epsilon)$, choosing ϵ such that the errors (which are of $O(\epsilon)$) are sufficiently small. In studying the limiting cases analytically, the full boundary conditions to be applied are

$$y(0) = 0, \quad t(1) = 0, \quad y(1) = h, \quad \theta(1) = \operatorname{arccot}(2kh). \tag{3.10}$$

3.2 Limiting Cases

Due to the complexity and nonlinearity of the governing equations, we begin with the limiting cases which allow us to find some analytical solutions, or otherwise simpler numerical computations. These asymptotic results give us a preliminary idea as to the validity of the model as well as allowing us to check our numerical simulation for the general case. In the real-life physical process, it is unlikely that a particular cylinder will contain both extreme limiting cases, as an increase in angular velocity and thus Centrifugal force, will give an increase in aerodynamic forcing and viscous drag. However, estimates of the size of the physical parameters involved for the three drums found in the revolving flat card suggest that κ lies in the range $(10^{-2}, 10)$ so that both the limits are potentially of interest.

3.2.1 Constant θ

We re-write (2.60) - (2.62) with constant θ to get,

$$\frac{dt}{ds} + \kappa y \cos\theta + \sin\theta = 0, \tag{3.11}$$

$$-2\kappa y \sin\theta + \cos\theta = 0, \tag{3.12}$$

$$\frac{dy}{ds} - \sin\theta = 0. \tag{3.13}$$

By integrating and using the boundary conditions for t and y, it is clear that there are only two limits in which $\theta =$ constant is admissible: either $\kappa = 0$, $\theta = \frac{\pi}{2}$ or $\kappa = \infty$, $\theta = 0$. These are shown in figure 3.2.

We can see from (3.11) - (3.13) that $y = 0$, $t = 0$ corresponds to $\theta = 0$, and $y(s) = s$, $t(s) = 1 - s$ corresponds to $\theta = \frac{\pi}{2}$. In one case the straight thread lies flat on top of the drum. This is equivalent to having no Centrifugal force, and the lack of tension in the fibre is due to the fact that the far field velocity $\mathbf{U} = \mathbf{0}$, at the solid boundary $y = 0$. The fibre in the model does not effect the 'outer' flow and the model treats the fibre as if it is part of the wall or an infinitesimal layer lying on top of the wall. In section 3.2.2 a perturbation method will be used to give a nearly flat fibre shape, i.e. where the viscous drag is the dominating body force. The other θ constant solution, is equivalent to having no drag, and we shall also look at this situation in more depth using perturbation expansions in section 3.2.3.



Figure 3.2: Two cases for constant θ

3.2.2 Small drag: $0 < \kappa \ll 1$

A regular perturbation expansion in powers of κ:

$$t(s) = \sum_{n=0}^{\infty} \kappa^n t_n(s), \quad y(s) = \sum_{n=0}^{\infty} \kappa^n y_n(s), \quad \theta(s) = \sum_{n=0}^{\infty} \kappa^n \theta_n(s) \tag{3.14}$$

is used to analyse the behaviour of the fibre when rotational forces dominate. Substituting these expansions into (2.60) - (2.62) the leading order terms satisfy,

$$t_0' + \sin\theta_0 = 0, \quad t_0\theta_0' + \cos\theta_0 = 0, \quad \text{and} \quad y_0' - \sin\theta_0 = 0. \tag{3.15}$$

with boundary conditions

$$y_0(0) = 0, \quad t_0(1) = 0, \quad y_0(1) = h, \quad \theta_0(1) = \frac{\pi}{2} \tag{3.16}$$

Manipulating (3.15)

$$\left(\frac{\cos\theta_0}{\theta_0'}\right)' = \sin\theta_0, \tag{3.17}$$

and then,

$$\frac{\theta_0''}{(\theta_0')} + 2\theta_0' \tan\theta_0 = 0. \tag{3.18}$$

The general solution is $\theta_0 = \arctan(As + B)$, A and B are integrating constants, and applying the boundary conditions (3.16) we find the only admissible solution is $\theta_0 = \frac{\pi}{2}$, and the corresponding tension $t_0 = 1 - s$ and $y_0 = s$ as found in section 3.2.1. The boundary conditions,

$$t(1) = 0, \quad y(1) = h, \quad \theta(1) = \frac{\pi}{2} - 2h\kappa + \frac{8(h\kappa)^3}{3} + O(\kappa^5), \tag{3.19}$$

are expanded asymptotically in κ. By inspection, the expansions take the form

$$\theta \sim \frac{\pi}{2} + \kappa\theta_1 + \kappa^3\theta_3 + \dots \tag{3.20}$$

$$t \sim 1 - s + \kappa^2 t_2 + \kappa^4 t_4 + \dots \tag{3.21}$$

$$y \sim s + \kappa^2 y_2 + \kappa^4 y_4 + \dots \tag{3.22}$$

and hence

$$h \sim 1 + \kappa^2 h_2 + \kappa^4 h_4 + \dots . \tag{3.23}$$

Substituting these into the equations (2.60) - (2.62) and the boundary conditions (3.19) we can solve explicitly for the coefficients as functions of s:

$$\theta_1 = -(s+1), \quad t_2 = \frac{s^2}{2} + s - \frac{3}{2}, \quad y_2 = -\frac{s}{6}(s^2 + 3s + 3). \tag{3.24}$$

These have been plotted in figure 3.3.

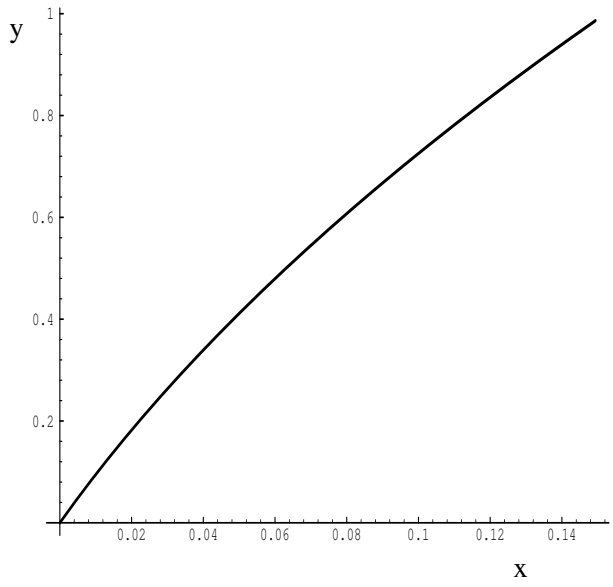


Figure 3.3: A graph plotting the fibre displacement with $\kappa = 0.1$.

3.2.3 Small centrifugal force: $\kappa \gg 1$

It is expected that tension in the fibre will react with, and thus balance, the body forces in the system. Due to the viscous drag dominating such forces it would be more

appropriate to scale the tension T with drag, as opposed to the centrifugal force in the original governing equations (2.60) - (2.60). Hence, we find,

$$\frac{d\tilde{t}}{ds} + y\cos\theta + \frac{1}{\kappa}\sin\theta = 0, \tag{3.25}$$

$$\tilde{t}\frac{d\theta}{ds} - 2y\sin\theta + \frac{1}{\kappa}\cos\theta = 0, \tag{3.26}$$

$$\frac{dy}{ds} - \sin\theta = 0, \tag{3.27}$$

where $t = \kappa\tilde{t}$ and κ is as defined previously as $\kappa = \frac{Dl}{F}$. Now, $\xi = \frac{1}{\kappa}$ is small and we proceed with an asymptotic analysis.

Asymptotic expansions

A regular perturbation expansion in $\xi^{\frac{1}{2}}$ is chosen after various balances between terms in the governing equations are analysed:

$$t(s) = \sum_{n=0}^{\infty} \xi^{n/2} t_n(s), \quad y(s) = \sum_{n=0}^{\infty} \xi^{n/2} y_n(s), \quad \theta(s) = \sum_{n=0}^{\infty} \xi^{n/2} \theta_n(s). \tag{3.28}$$

Substituting these into (3.25) - (3.27) we find the known θ constant solution, $\theta_0 = 0$, $y_0 = 0$ and $t_0 = 0$, satisfies the leading-order equations, also by considering (2.53) we know that $x = s + O(\xi)$. The first order-terms are,

$$t_1\theta_1' - 2y_1\theta_1 + 1 = 0, \tag{3.29}$$

$$t_1' + y_1 = 0, \tag{3.30}$$

$$y_1' = \theta_1. \tag{3.31}$$

Expanding the boundary conditions in terms of the perturbation expansion gives,

$$y_1(0) = 0, \quad t_1(1) = 0, \quad 2y_1(1)\theta_1(1) = 1. \tag{3.32}$$

Solution of the first-order equations

We have boundary-value problem for a nonlinear third order ordinary differential equation. A shooting method is used, which consists of a finite difference schemes to solve an initial-value problem with a guess for $y(1)$. Then a Secant algorithm finds the appropriate initial condition at $y(1)$ that corresponds to $y(0) = 0$, see Conte and De Boor[7]. We perform the integration and root-finding using Mathematica, see Appendix A.1.

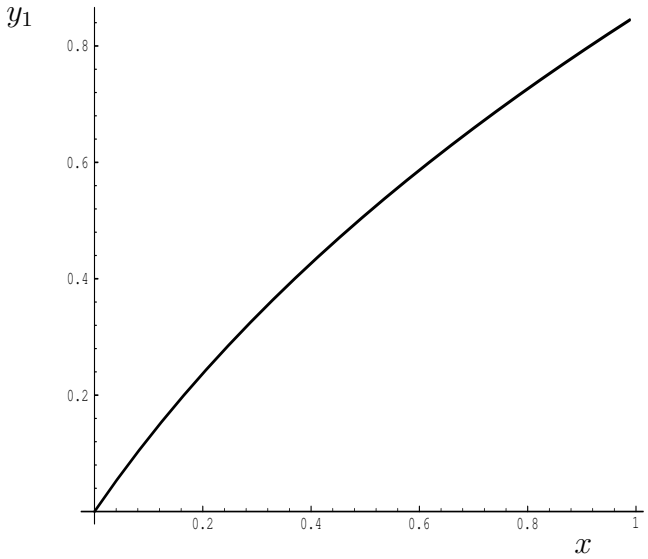


Figure 3.4: A graph of the first-order fibre displacement.

3.3 General κ

One numerical approach to solve the full governing equations would be similar to method used for finding the first order equations from the previous section 3.2.3. The equations (2.60) - (2.62) are posed with the following boundary conditions,

$$t(1) = \epsilon \frac{1 + 2(h\kappa)^2}{\sqrt{1 + 4(h\kappa)^2}}, \tag{3.33}$$

$$\theta(1) = \operatorname{arccot}(2\kappa h), \tag{3.34}$$

$$y(1) = h, \tag{3.35}$$

derived from (3.7) - (3.9). We guess h, then solve the differential equations for some very small value of ϵ. A root solve is then used to vary h in order satisfy $y(0) = 0$.

3.3.1 Reformulation of problem

Alternatively, we rescale:

$$y = h\Upsilon, \quad t = h\tau, \quad \kappa = \frac{\lambda}{h}, \quad \epsilon = \delta h \tag{3.36}$$

which uses the autonomy of s in (2.60) - (2.62). These give the following formulation of the equations,

$$\frac{d\tau}{d\Upsilon} = -(1 + \lambda\Upsilon \cot\theta), \tag{3.37}$$

$$\frac{d\theta}{d\Upsilon} = \frac{1}{\tau}(2\lambda\Upsilon - \cot\theta), \tag{3.38}$$

with the boundary conditions evaluated at $\Upsilon(1) = 1$,

$$\left.\begin{array}{r} \tau(\Upsilon) = \delta\frac{1+2\lambda^2}{\sqrt{1+4\lambda^2}} \\ \theta(\Upsilon) = \operatorname{arccot}(2\lambda) \end{array}\right\} \quad \text{at} \quad \Upsilon = 1. \tag{3.39}$$

Note that since $h < 1$, $0 < \delta \leq \epsilon \ll 1$.

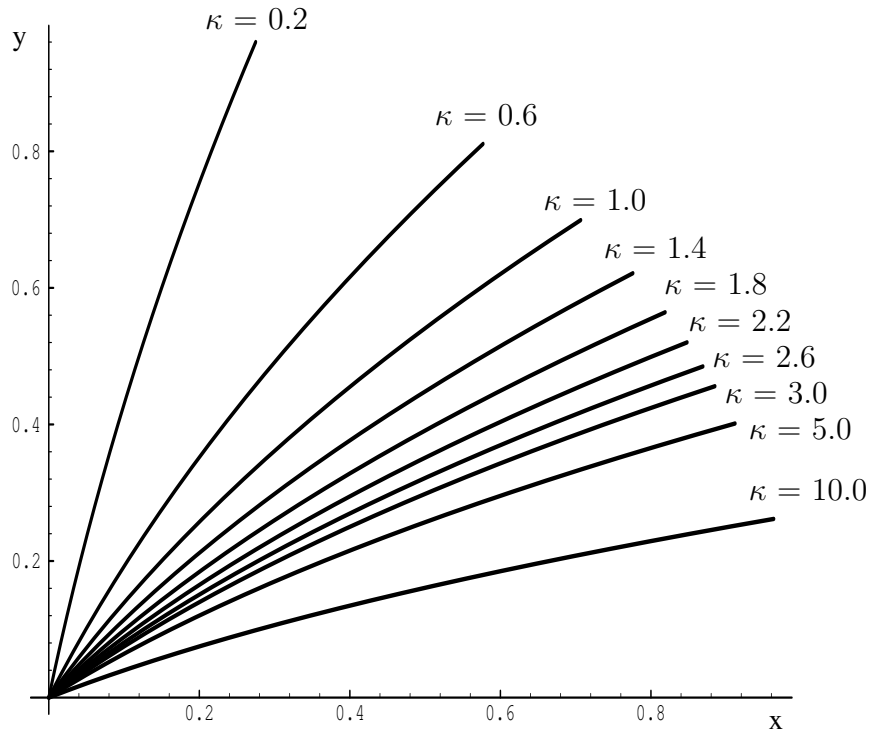


Figure 3.5: Fibre displacements for varying κ

For a given λ, we solve the new system (3.37) - (3.39) as an initial-value problem for $\Upsilon \in [0, 1)$. The condition $y(0) = 0$ is now an equation for h in terms of $\theta(\Upsilon)$ from our numerical solutions, namely

$$h = \frac{1}{\int_0^1 \operatorname{cosec}[\theta(\varsigma)]d\varsigma}. \tag{3.40}$$

Now, rescaling x with $x = h\chi$ we have,

$$\frac{d\chi}{d\Upsilon} = \cot\theta. \tag{3.41}$$

From these, (3.40) and (3.41), we can find the shape of the thread parametrically, using

$$y = h\Upsilon, \tag{3.42}$$

$$x = h\int_0^{\Upsilon} \cot[\theta(\varsigma)]d\varsigma. \tag{3.43}$$

In figure 3.5 we show the fibre profiles for varying κ. All the numerical computations have been done using Mathematica, see Appendix A.2.

We can also attain a lot of information about the system by plotting the height h at the end of the fibre from the drum surface, against $\kappa = \frac{\lambda}{h}$, see figure 3.6. This should enable us to determine whether the fibre is likely to be caught by a passing hook.

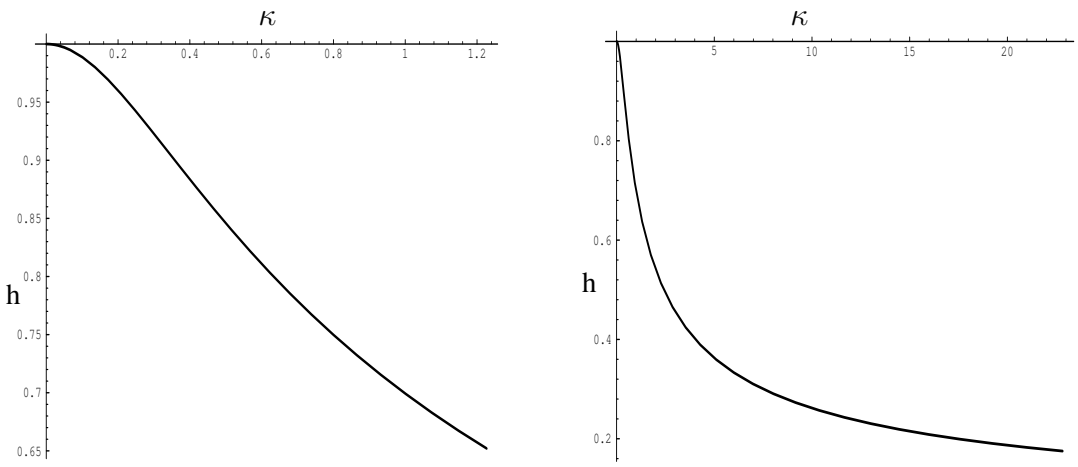


Figure 3.6: The height as a function of the nondimensional constant κ

3.3.2 Comparison of numerical and asymptotic solution

To check our numerical solutions, we compare them to the solutions of the two limiting cases of κ small and κ large from sections 3.2.2 and 3.2.3 respectively. For κ large we rescaled with (3.36) and found a numerical solution to the resulting leading order problem. One prediction of the analysis was that $h \sim 0.8448/\sqrt{\kappa}$ as $\kappa \to \infty$ and in figure 3.7 we show that indeed $h = O(1/\sqrt{\kappa})$ as $\kappa \to \infty$. In figure 3.8 we compare the leading order asymptotic fibre shape with the full numerical solution, with $\kappa = 10$ and find that the two are in good agreement.

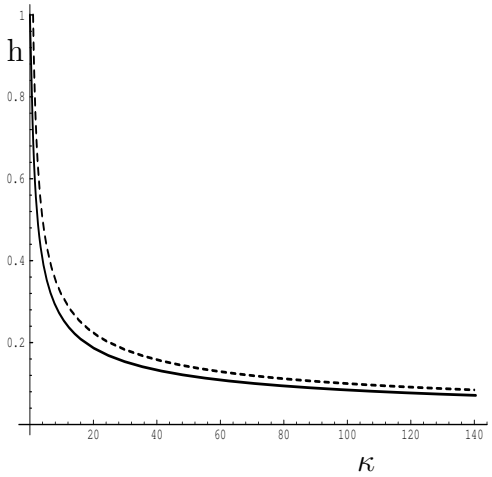


Figure 3.7: The h against κ, with $\frac{1}{\sqrt{\kappa}}$ the dotted line

We compare our small κ expansions with the full solution in figure 3.9, setting $\kappa = 0.1$. Again the agreement is excellent, so we can be satisfied with our computations.

3.4 The Hook Problem

The force at the fixed end can be derived from our calculations in section 3.3. In terms of tension in Cartesian components it reads

$$T(0)\begin{pmatrix} \cos[\theta(0)] \\ \sin[\theta(0)] \end{pmatrix}.$$

If the hook has an angle of attack ζ as in figure 3.5 then the friction force F and the normal force N are defined as follows,

$$\mathrm{F} = T(0)\cos[\theta(0) - \zeta], \tag{3.44}$$

$$\mathrm{N} = T(0)\sin[\theta(0) - \zeta]. \tag{3.45}$$

The fibre will slip if

$$\left|\frac{\mathrm{F}}{\mathrm{N}}\right| > \mu_s, \tag{3.46}$$

where μ_s is the fiction coefficient between the hook and the fibre tip. It must be stated that there is the assumption that the hydrodynamic effects caused by the hook can be ignored. As our asymptotic approximation for the drag is only to leading order, this

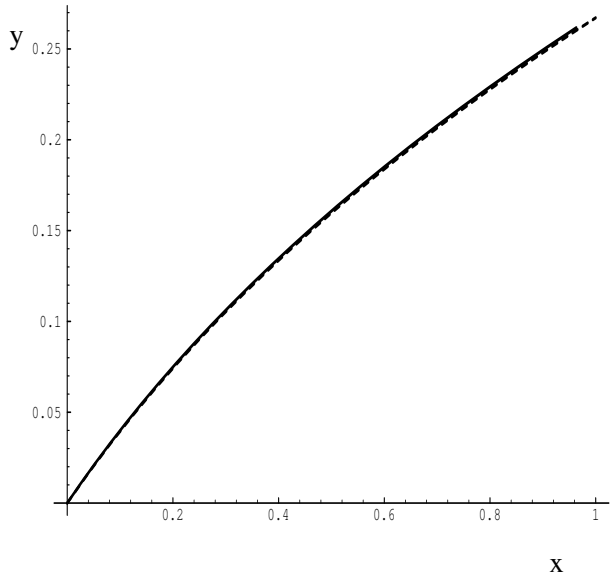


Figure 3.8: Fibres for $\kappa = 10$, $\epsilon = 10^{-5}$, the asymptotic solution is the dotted line.

assumption is reasonable: the interaction between two particles or between a particle with a wall is found to be first order, see Cox [8]. If the interface between the hook and the fibre, see figure 3.10, is reasonably high (the height is not small compared to the fibre length), then we would have to adjust our governing equations with a different Shear flow. The no-slip condition on the far field flow of the fluid velocity would be significantly lower than the interface between hook and fibre, resulting in a comparatively higher viscous drag contribution.

We see that where the angle of attack ζ is obtuse, the fibre seems most stable when the angle at the joining point between hook and the fibre tangent is orthogonal, and this is shown in figure 3.11. In the case where ζ is acute, see figure 3.12, the sharper angles correspond to stronger holding forces. The singularity in figure 3.13, is due to the fibre tangent having an angle at the fibre-hook interface being the same as the angle of attack of the hook. This means that there is no holding force orthogonal to the hooks surface, and the $\frac{F}{N}$ term becomes singular.

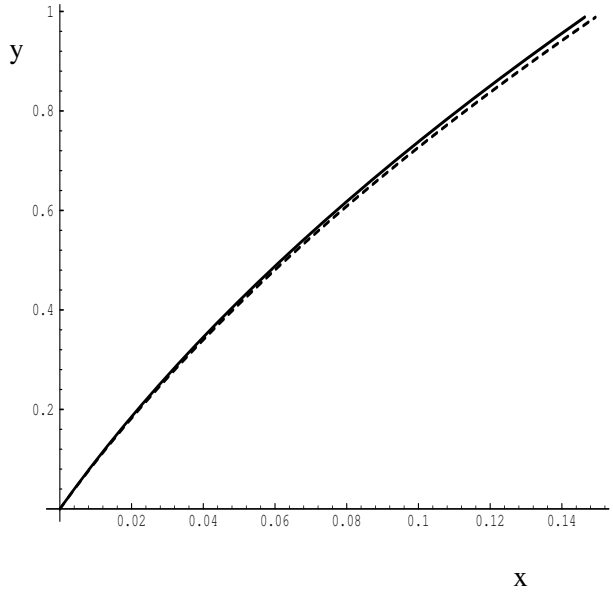


Figure 3.9: Fibres for $\kappa = 0.1$, $\epsilon = 10^{-5}$, the asymptotic solution is the dotted line.

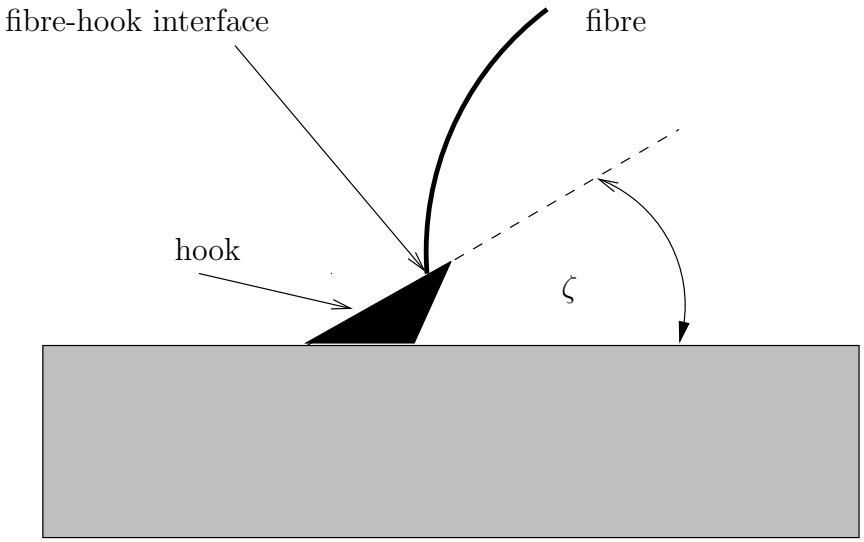


Figure 3.10: A diagram of the hook and fibre

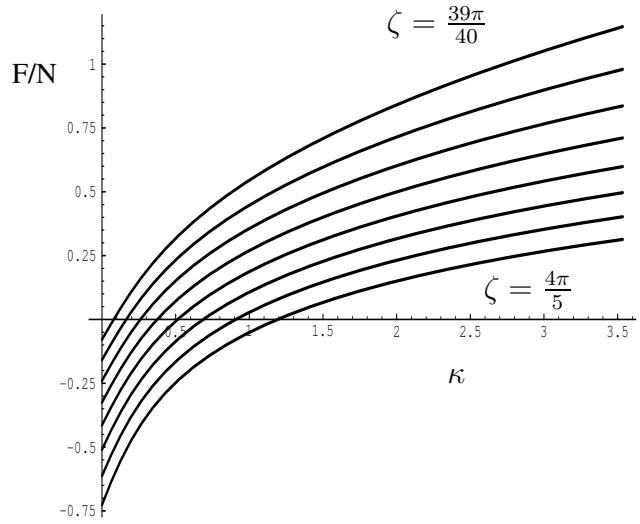


Figure 3.11: F/N plotted against κ for varying ζ, where ζ is incremented in by $\frac{\pi}{40}$.

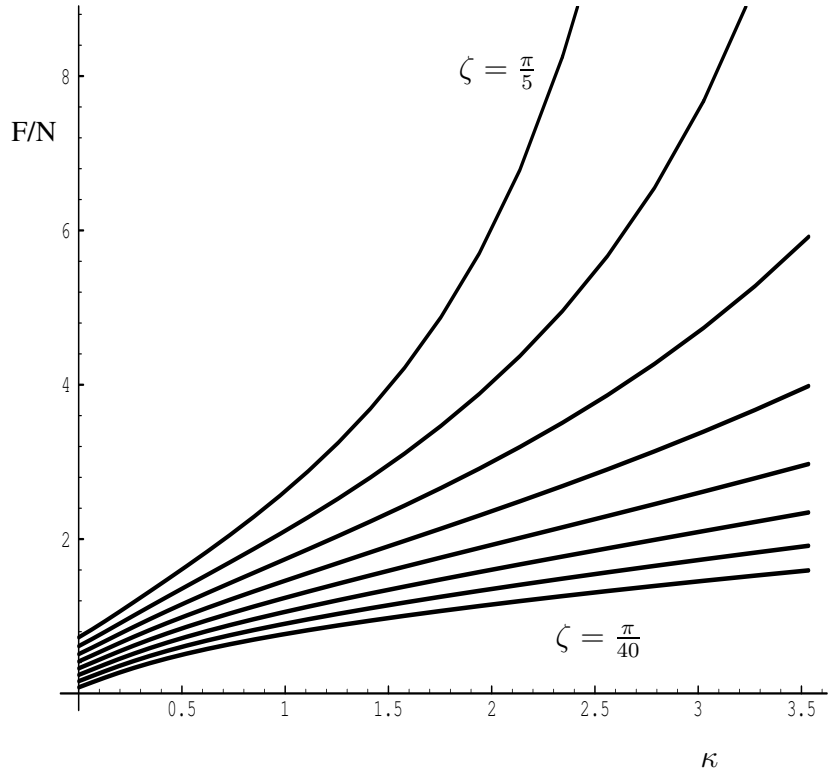


Figure 3.12: F/N plotted against κ for varying ζ, where ζ is incremented in by $\frac{\pi}{40}$.

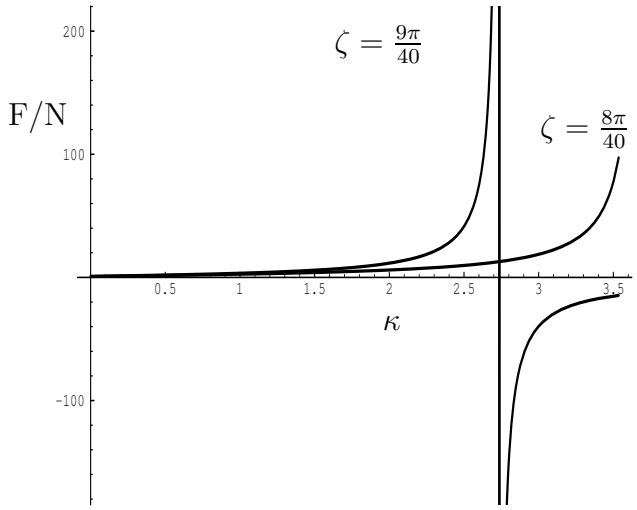


Figure 3.13: F/N plotted against κ, for larger angles of attack ζ.

Chapter 4

Conclusion

We have given a basic description of the various steps within the carding procedure. Of these we concentrated on the analysis of a single fibre attached to rotating cylindrical drum. We included viscous drag, a centrifugal body force and the effects of a varying angle between the drum and a metal wire, to which one end of the fibre is fixed. This regime is relevant to both stripping and carding, and the analysis enables us to estimate the forces required to hold the fibre on the wire in either case.

The model was derived rigorously using Newton's laws and the classical hydrodynamic equations for a Newtonian fluid. The viscous drag on a fibre was found to leading order using matched asymptotic expansions, assuming that the Reynolds number (on the scale of a single fibre) is small. The resulting model constitutes a set of three coupled autonomous ordinary differential equations for the tension in the fibre, the height of the fibre from the drum, and θ, the angle between the tangent to the fibre and the horizontal, as a function of arc length. The equations have a single dimensionless parameter κ, which is a ratio between the viscous drag and centrifugal force. There are two boundary conditions, of which one is singular, and by eliminating the singularity we found a third condition that makes the system well-posed.

We performed a local analysis of the aforementioned singularity, which gave us asymptotic boundary conditions that were needed for the numerical simulation. In the general case the system was reduced to a boundary-value problem for two non-autonomous nonlinear ordinary differential equations. By a crafty rescaling we simplified this to an initial value problem. We solved this numerically to find the fibre shape as a function of κ. This was compared to two limiting cases for κ, where simplifications to the original governing equations could be made using perturbation analysis.

We found these to be consistent, which supports the validity of the numerical results.

Most importantly in practice, our model can be used to predict the distance the fibre sticks out from the drum and the force that is required to hold the fibre in place, and how both of these depend on κ. The former could tell us whether a fibre is likely to be stripped off by a passing hook, and from the latter we can estimate whether the fibre will slip off a wire with a given angle of attack.

There are a number of ways in which one could continue with this particular problem. A stability analysis on the steady state solution would prove useful, and would necessitate the inclusion of inertia effects. Other fluid flows may be used to simulate the more interactive regions of the process. Different body forces could be employed. For example if the fibre length is comparable with the drum radius, then the centrifugal force takes a more complicated form. Also different flow regimes from Couette flow could be considered. The asymptotic expansions for drag only considered leading-order terms, and so the inclusion of higher-order effects would give a more accurate model. Such effects would be particularly important in physical situations like a two-fibre problem or the interaction with a wall, see Cox [8]. Full time-evolution equations would give the opportunity to consider a variety of initial fibre shapes, and give a more detailed description of the forces required to hold a fibre to a hook. A starting point for such work is the paper by Gradon and Podgorsky [13]. All the aforementioned modifications do not change the material of the fibre itself. Introducing bending stiffness, elasticity and the possibility of naturally curved fibres would certainly broaden the application of this one-fibre study.

There are a number of other elements in Carding that could be posed mathematically. A mass of fibres in a fluid can be modelled with a two-continuum model, where one of the continua is a mixture of fibres and air and the other is just air. This would follow the work of Terrill [25], who applied these techniques to the spinning process. Other approaches could consider a discrete many-body problem, modelled with stochastic (ito) calculus or other statistical methods, and allow for noise in the system that comes from the turbulent fluid flow, or interactions with a large number of fibres, and other irregularities within the machine. We could develop a macroscopic model like Cherkassy [5], which considers input and output governed by process function.

The present work is the first step on the long road to the understanding of the carding process, and thence of many other textile processes.

Appendix A

Computations in Mathematica

A.1 Differential Equations: a shooting method

A method to solve the system of first order differental equations from: (3.29) - (3.31) with (3.32).

```
f[x_,e_] := NDSolve[{t[s] theta'[s] - 2 y[s] theta[s] + 1 == 0,
t'[s] + y[s] == 0, y'[s] == theta[s], t[1] == e, y[1] == x, theta[1]
== 1/(2 x)},theta ,t,y},{s,0,1}][[1]]
g[x_,e_] := Module[ {a}, a = f[x,e]; y[0] /. a]
fr[e_, guess1_ , guess2_] := FindRoot[ g[x,e] == 0, {x,{guess1,guess2}}]
```

A.2 Differential Equations: the full equations

A method to solve the full governing equations, (3.37), (3.38), and (3.39).
Solve the differential equation:

```
f[lambda_,delta_] := NDSolve[ {tau'[y] == -(1 +
y lambda Cot[theta[y]]), theta'[y] == (1/tau[y]) (2 y lambda -
Cot[theta[y]]), tau[1] == (1 + 2 (lambda^ 2)) (delta) / (1 +
4 (lambda^ 2))^ (1/2), theta[1] == ArcCot[ 2 lambda]},
{tau, theta}, {y,0,1} ][[1]]
```

Find $\frac{1}{h}$:

```
g[Y_,lambda_,delta_] := Module[{a}, a = f[lambda,delta];
```

```
NIntegrate[Csc[theta[y] /. a], {y,0,Y}] ]
```

Plot h against κ:

```
kh[delta_,lambdamax_] := ParametricPlot[ {1/g[1,lambda,delta],
lambda g[1,lambda,delta]}, {lambda,0,lambdamax}]
```

Plot the fibres, first finding the x from the theta arc length variable:

```
X[Y_,lambda_,delta_] := Module[{a}, a = f[lambda,delta];
NIntegrate[Cot[theta[y] /. a], {y,0,Y}] ]
```

The fibre plotting function:

```
fibre[lambda_,delta_] := ParametricPlot[ {(1/(g[1,lambda,delta]))
X[Y,lambda,delta], Y (1/(g[1,lambda,delta]))}, {Y,0,1} ]
```

A.3 Differential Equations: the hook

For the release approximation:

```
FN[lambda_,zeta_,delta_] := Module[{a}, a = f[lambda,delta];
N[Cot[(theta[0] /. a) - zeta]] ]
```

Plot against F/N against κ:

```
lambdaFN[zeta_,delta_,lambdamax_] := ParametricPlot[ {lambda(g[1,lambda
,delta]),FN[lambda,zeta,delta]},{lambda,0,lambdamax} ]
```

Bibliography

[1] G. K. Batchelor
An Introduction to Fluid Dynamics
Cambridge University Press, 1967

[2] G. K. Batchelor
Slender-body theory for particles of arbitrary cross-section in Stokes flow
Journal of Fluid Mechanics, **44**, 1970

[3] Y. A. Baturin
The load of the surfaces and the proportion of fibre transferred between the surfaces
Technology of Textile Industry, **4**, 1964

[4] R. N. Barshinger
Stokes-flow past a thin oblate body of revolution - axially incident uniform-flow
SIAM Journal of Applied Mathematics, **44**, 1984

[5] A. Cherkassky
A two-dimensional mathematical model of the carding process
Textile Research Journal, **64**, 1994

[6] A. T. Chwang and T. Yao-Tsu Wu
Hydromechanics of low Reynolds-number flow. Part 2. Singularity methods for Stokes flows
Journal of Fluid Mechanics, **67**, 1975

[7] S. D. Conte and C. De Boor
Elementary Numerical Analysis: an algorithmic approach
McGraw-Hill, 1980

[8] R. G. Cox
The motion of long slender bodies in a viscous fluid. Part 1. General theory
Journal of Fluid Mechanics, **44**, 1970

[9] Crosrol Ltd
A Theory of Carding

[10] T. Dabros
A singularity method for calculating hydrodynamic-forces and particle velocities in low-Reynolds-number flows
Journal of Fluid Mechanics, **156**, 1985

[11] P. G. Drazin and W. H. Reid
Hydrodynamic Stability
Cambridge University Press, 1981

[12] L. Gradon, A. Podgorski, and P. Grzybowski
Deposition of flexible and stiff fibrous particles
Journal of Aerosol Science, **20**, 1989

[13] L. Gradon and A. Podgorski
Flexible fibrous particle behaviour in the carrier gas flow around cylindrical obstacle
Chemical Engineering Science, **45**, 1990

[14] E. J. Hinch
The distortion of a flexible inextensible thread in a shearing flow
Journal of Fluid Mechanics, **74**, 1976

[15] J. B. Keller and S. I. Rubinow
Slender-body theory for slow viscous flow
Journal of Fluid Mechanics, **75**, 1976

[16] R. E. Khayat and R. G. Cox
Inertia effects on the motion of long slender bodies
Journal of Fluid Mechanics, **209**, 1989

[17] H. W. Liepmann and A. Roshko
Elements of Gas Dynamics
John Wiley & Sons, 1957

[18] M. J. Lighthill
Mathematical Biofluiddynamics.
SIAM, 1975

[19] J. T. Marsh
Textile Science, An Introductory Manual
Chapman & Hall, 1953

[20] A. Podgorski and L. Gradon
Motion and deposition of fibrous flexible particles in laminar gas flow through a pipe
Journal of Aerosol Science, **21**, 1990

[21] L. Rosenhead (editor)
Laminar Boundary Layers
Oxford University press, 1963

[22] S. Sarkar and J. L. Lumley
A continuum two-field theory for dilute fibre suspensions
Acta Mechanica, **80**, 1989

[23] E. S. G. Shaqfeh and D. L. Koch
The effect of hydrodynamic interactions on the orientation of axisymmetric particles flowing through a fixed bed of spheres or fibres
Physics of Fluids, **31**, 1988

[24] E. S. G. Shaqfeh and G. H. Fredrickson
The hydrodynamic stress in a suspension of rods
Physics of Fluids A, **2**, 1989

[25] E. L. Terrill
Mathematical modelling of some spinning processes
D. Phil. Thesis, University of Oxford, 1990

[26] G. K. Youngren and A. Acrivos
Stokes flow past a particle of arbitrary shape: a numerical method of solution
Journal of Fluid Mechanics, **69**, 1975